PHYSICAL REVIEW D **94,** 061901(R) (2016)

New dynamical instability in asymptotically anti–de Sitter spacetime

Umut Gürsoy,[1] Aron Jansen,[1] and Wilke van der Schee[2]

[1]*Institute for Theoretical Physics and Center for Extreme Matter and Emergent Phenomena, Utrecht University, Leuvenlaan 4, 3584 CE Utrecht, Netherlands*

[2]*Center for Theoretical Physics, MIT, Cambridge, Massachusetts 02139, USA*

(Received 12 May 2016; published 16 September 2016)

We present fully dynamical solutions to Einstein-scalar theory in asymptotically anti–de Sitter spacetime with a scalar potential containing particularly rich physics. Depending on one parameter in the potential, we find an especially interesting regime, which exhibits a dynamically unstable black brane, already at zero momentum, while nevertheless having positive specific heat. We show this using the nonlinear dynamics and give a clear interpretation in terms of the spectrum of linearized perturbations. Our results translate directly to their dual strongly coupled nonconformal field theories, whereby we in particular provide two mechanisms to obtain equilibration times much larger than the inverse temperature.

DOI: 10.1103/PhysRevD.94.061901

I. INTRODUCTION

Holography has led to crucial qualitative lessons for the physics of real-time dynamics and equilibration in strongly coupled quantum theories, such as the fast applicability of hydrodynamics, within a time of $1/T$, with T being the temperature of the plasma [1–4]. These studies were mostly performed in a scale invariant setting, where the $1/T$ scaling is automatic. Much richer physics can be expected for theories without scale invariance or relativistic symmetry, which is an active topic of current research both in relation to quark-gluon plasma [5–12] and condensed matter systems [13–15]. In this paper, we present such a new lesson, where we find stationary phases which display a dynamical instability at zero momentum, whereby the time scale of the instability can be much larger than the inverse temperature.

Einstein-scalar theory in the context of nonconformal holographic QCD was first introduced in Refs. [16,17] (see also Ref. [18]). In this paper, we follow Refs. [19,20], which introduced a simple potential that could mimic the thermodynamics of QCD as in Refs. [16,17] but differs from the latter in the small ϕ asymptotics. Our potential contains an exponent γ that controls the deviation of the dual field theory from the conformal limit $\gamma = 0$. In particular, it was shown in Ref. [21] that the dual theory exhibits a confinement-deconfinement transition for the choice $\gamma \geq 4/3$. However, most of the detailed analysis focused on the particular case of $\gamma = 4/3$, which is the most realistic choice for the QCD phenomenology [22].

In this paper, we initiate a detailed study of the regime $\gamma > 4/3$ by solving Einstein-scalar equations of motion both in a time-independent and a time-dependent setting to determine respectively the thermodynamics and the process of thermalization in the corresponding dual field theory. We discover a new critical value $\gamma_c \approx 1.65$ beyond which a new, qualitatively different regime arises. This value depends on the mass of the scalar that corresponds to the scaling dimension of the scalar operator Δ, and the quoted value is for $\Delta = 3$. For smaller γ, it is known that there is a minimum temperature, at fixed source, above which there is a large, stable branch and an unstable branch which has negative specific heat and a vanishing entropy for large temperature. For larger γ, we find that both branches at the minimum temperature have positive specific heat. Interestingly, the solution with smaller black brane area still has growing entropy for large T but is nevertheless dynamically unstable and hence contains an exponentially growing mode. Lastly, as the temperature goes toward the minimum temperature, both solutions coalesce, whereby the relaxation time diverges. We illustrate all these features by tuning our initial conditions such that the evolution first relaxes onto the unstable black brane solution, after which it decays into the stable black brane.

We hence provide two mechanisms to violate the typical $\mathcal{O}(1/T)$ scaling of the equilibration time. First, as mentioned, it is possible to increase the source to its maximum value, or equivalently decrease the temperature to its minimal value, where the equilibration time diverges. Second, at smaller sources, it is possible to fine-tune the initial conditions such that the evolution stays at the unstable time-independent solution for a time $\gg 1/T$.

Our results also provide an interesting addition to the literature on the instability of black branes [23]. In particular, it is different from a Gregory-Laflamme type instability [24]. These types of instabilities are often present in black rings and black branes in more than four dimensions and involve the breakup of the ring or brane into smaller parts, which can be thermodynamically favorable. Curiously, the thermodynamics of black holes crucially relies on Hawking's computation [25], which requires quantum mechanics. It is hence not obvious that the classical Einstein equations would contain a dynamical instability, if a thermodynamic instability is present (see, however, Ref. [26]). Nevertheless, a black brane always contains a dynamical instability if a thermodynamic instability is present, as conjectured by Gubser and Mitra in

Refs. [27,28] (see also Refs. [29–31]) and recently proved in Ref. [32].

Our example is reminiscent of the models studied in Ref. [33]. This reference also has hairy black holes in Einstein-scalar theory, which are not unique when specifying all conserved charges. They note that these nonunique stationary solutions can be unstable to flow toward other solutions. Since this does not necessarily involve conserved charges, this instability can also occur at zero momentum and with positive specific heat, such as the example presented here in a fully nonlinear dynamical setting [34].

II. MODEL AND RESULTS

Our confining model is given by the Einstein-scalar action

$$\mathcal{S}=\frac{1}{16\pi G_{d+1}}\int d^{d+1}x\sqrt{-g}\left(R-\frac{4}{3}(\partial\Phi)^2+V(\Phi)\right), \quad (1)$$

which includes a scalar field dual to a scalar operator $\mathcal{O}$ with scaling dimension Δ. We follow Refs. [19,20] and take

$$V(\Phi)=d(d-1)\left(\left(\frac{4\Delta(d-\Delta)}{3d(d-1)}-\frac{\gamma^2}{2}\right)\Phi^2+\cosh(\gamma\Phi)\right), \quad (2)$$

which near $\Phi=0$ reads

$$V(\Phi)=(d-d^2)+\frac{4}{3}\Phi^2(\Delta^2-d\Delta)+O(\Phi^4), \quad (3)$$

such that we have a negative cosmological constant with $L_{\mathrm{AdS}}=1$, and the mass of the scalar is independent of the value of the free parameter γ. In this paper, we present results for $d=4$ and $\Delta=3$. In order to solve dynamical simulations, it is convenient to use the characteristic formulation of general relativity [1,35,36], which is achieved by using a metric ansatz,

$$ds^2=-\frac{2}{z^2}dtdz-Adt^2+S^2d\vec{x}^2, \quad (4)$$

whereby we study homogeneous solutions which only depend on time t and anti–de Sitter (AdS) radial coordinate z (the AdS boundary corresponds to $z=0$). The equations of motion following from (1) are written down in i.e. Ref. [5] and lead to a near-boundary expansion for Φ and A as

$$\begin{aligned}\Phi(z,t)=&\,jz+jz^2\eta(t)\\&+z^3\left(f_3(t)+\frac{1}{72}(32-27\gamma^4)j^3\log(z)\right)\\&+O(z^4),\end{aligned} \quad (5)$$

$$\begin{aligned}A(z,t)=&\,\frac{1}{z^2}-\frac{2\eta(t)}{z}+\left(-\frac{4j^2}{9}+2\eta'(t)+\eta(t)^2\right)\\&+z^2\left(a_4(t)+\frac{1}{162}(27\gamma^4-32)j^4\log(z)\right)\\&+O(z^3),\end{aligned} \quad (6)$$

where j is a time-independent source for the scalar, $f_3(t)$ and $a_4(t)$ are the normalizable modes undetermined by the near-boundary analysis, and $\eta(t)$ is a gauge freedom left in (4), which we use to fix the apparent horizon at $r=1$. The normalizable mode $f_3(t)$ has dimension 3 and hence in principle scales as j^3 for fixed j/T. However, due to the anomalous logarithmic term in (5), $f_3(t)$ also includes a term $\frac{1}{72}(27\gamma^4-32)j^3\log(j)$. The expectation value of $\mathcal{O}$ can be obtained through holographic renormalization [5,37],

$$\langle\mathcal{O}\rangle=\frac{8f_3(t)}{3}+\left(\frac{8}{27}-\frac{\gamma^4}{2}\right)j^3, \quad (7)$$

where we again notice that this includes an anomalous term proportional to $j^3\log(j)$. As always, there is a scheme dependence in the renormalization procedure whereby finite counterterms can shift (7) without affecting the physics presented.

Lastly, we have to specify initial conditions. Both for numerics and for presentation, it is convenient to treat the near-boundary behavior of Φ analytically and hence define $\tilde{\Phi}(z,t)$ as

$$\begin{aligned}\Phi(z,t)\equiv&\,jz+jz^2\eta(t)+z^3\left(\tilde{\Phi}+\left(\frac{32}{72}-\frac{3}{8}\gamma^4\right)j^3\log(z)\right)\\&+\frac{3}{8}\left(\frac{32}{9}-3\gamma^4\right)j^3\eta(t)z^4\log(z)),\end{aligned} \quad (8)$$

where by construction $\tilde{\Phi}(0,t)=f_3(t)$, which leads directly with the expectation value of the scalar through Eq. (7). The initial conditions are then fully specified by $\tilde{\Phi}(z,0)$ for $\eta(0)=0$ together with $a_4(0)$.

During the evolution, we furthermore keep track of the spectrum of linearized perturbations around the metric with scalar field, the so-called quasinormal modes (QNM). We solved for the QNM spectrum by constructing gauge invariant observables from the linearized equations [38,39]. This is done by rewriting background and perturbations as in $\phi(z,t)=\phi_0(z)+e^{i\omega t}\delta\phi(z)$ and analogously for $g_{\mu\nu}$ in terms of

$$Z_\phi(z)\equiv\delta\phi(z)-\frac{\phi'(z)}{6S(z)S'(z)}(\delta g_{xx}(z)+\delta g_{yy}(z)+\delta g_{zz}(z)),$$

which is invariant under infinitesimal transformations $g_{\mu\nu}\to g_{\mu\nu}-\nabla_\mu\xi_\nu-\nabla_\nu\xi_\mu$ and $\phi\to\phi(z)-\nabla^\lambda(\phi_0(z)\xi_\lambda)$.

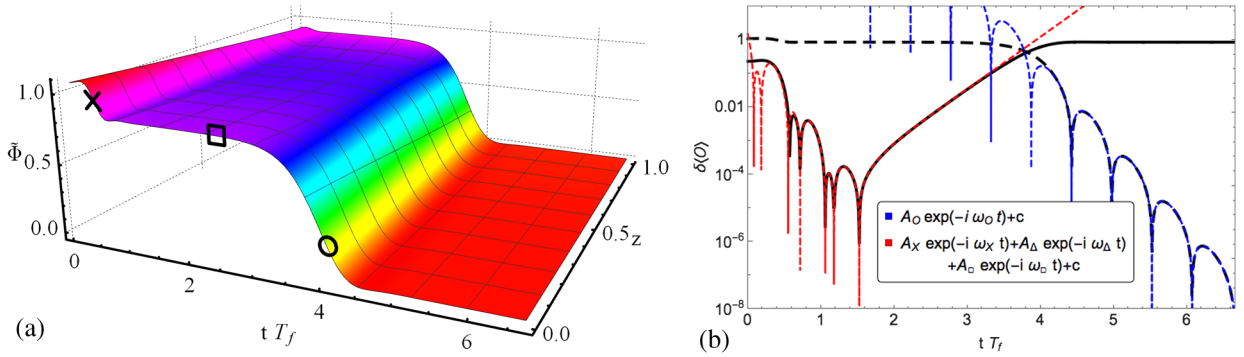

FIG. 1. (a) We show the dynamical solution for $\tilde{\Phi}$ [as in Eq. (8)] with initial conditions given by $j = 0.2$, $a_4(0) = -1$ and $\tilde{\Phi}(z,0) = 1.06822$ for the potential (2) with $\gamma = 4\sqrt{2}/3$. Interestingly, this evolution finds both an unstable and a stable solution. The dynamics hence goes through three regimes, as more clearly shown in (b). There, we show the difference $\delta\langle\mathcal{O}\rangle(t)$ between $\langle\mathcal{O}\rangle(t)$ and the equilibrium values $\langle\mathcal{O}\rangle(1.55/T_f)$ and $\langle\mathcal{O}\rangle(7/T_f)$ of the unstable and stable phases in solid and dashed black respectively. Both plots show time in units of the final temperature T_f. The system first equilibrates to the unstable phase, dominated by two QNMs of frequencies $(\omega_X, \omega_\Delta)/\pi T = (3.23 - 1.93i, -2.18i)$. After this, the unstable QNMs becomes dominant, and this mode grows exponentially with $\omega_\square/\pi T = 0.92i$. Lastly, this mode leaves the linear regime, and the solution finally rings down to the stable solution with $\omega_O/\pi T = 1.82 - 1.79i$.

At zero momentum, this satisfies a decoupled equation of the form

$$Z''_\phi(z) + F_1(\omega, z)Z'_\phi(z) + F_0(\omega, z)Z_\phi(z) = 0, \quad (9)$$

where F_0 and F_1 are lengthy functions of the background geometry [40]. We used spectral methods to solve the eigenvalue problem associated to (9) and hence obtain the QNM spectrum [41].

The main result is captured in Fig. 1(a), where we take $\gamma = 4\sqrt{2}/3$ [42], $j = 0.2$ and initial conditions $a_4(0) = -1$ and $\tilde{\Phi}(z,0) = 1.06822$. Strikingly, the time evolution of this initial profile goes through three phases. First, within a time of the inverse temperature, the system relaxes to a time-independent state. This time-independent state is, however, unstable, and after a time depending on how close the unstable state was reached the system relaxes again to the stable solution. We stress that we needed to fine tune our initial condition to remain at the unstable state for a long time, but apart from this fine-tuning, this phenomenon is fully generic, provided $\gamma \gtrsim 1.65$ [43].

In Fig. 1(b), the three regimes are shown more clearly. First, there is the decay to the unstable solution by the lowest two stable QNM of the unstable phase, which is dominant since we fine tuned the coefficient of the unstable QNM to be small. Then there is a semistationary period where this small coefficient grows exponentially. Finally, the solution exits the linear regime around the unstable solution and rings down in the linear regime around the stable solution. All three dominant modes are indicated in Fig. 2, as red QNMs around the unstable background (first phases) and around the stable background (blue). Note that the unstable QNM has a vanishing real part, which is required [23]. It is reassuring to see all QNMs of the stable and unstable solutions meet at $j = j_{\max}$. It is interesting that the lowest QNM of the stable phase crosses the second QNM to meet the stable partner of the unstable QNM of the unstable phase.

Interestingly, for a larger source, we find the same features, up to a maximum source $j_{\max}$, as illustrated in Figs. 2 and 3(a). At $j = j_{\max}$, the unstable and stable branches merge, and the lowest QNM of both solutions has $\omega = 0$. This then naturally gives rise to an overdamped relaxation toward the equilibrium solution, which we show in Fig. 3(b). Clearly, at this point, the thermalization takes asymptotically longer than the standard $1/T$ with T the

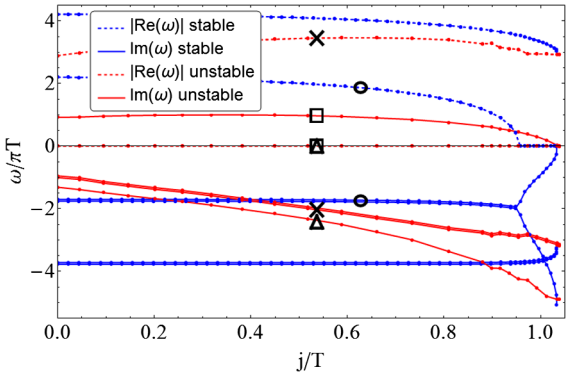

FIG. 2. We show the first two QNM of both the stable (blue) and unstable (red) solutions as a function of the source over the temperature. The unstable solution always contains a mode with a positive imaginary part (solid red), which goes to zero for the maximum source allowed. At this point, the stable solution also has a vanishing imaginary part, which corresponds to a diverging relaxation time. Interestingly, the lowest QNM of the stable phase has vanishing real part for $j/T > 0.95$, after which the imaginary parts separate. This is needed for the modes to meet at the maximum source, where both phases coalesce.

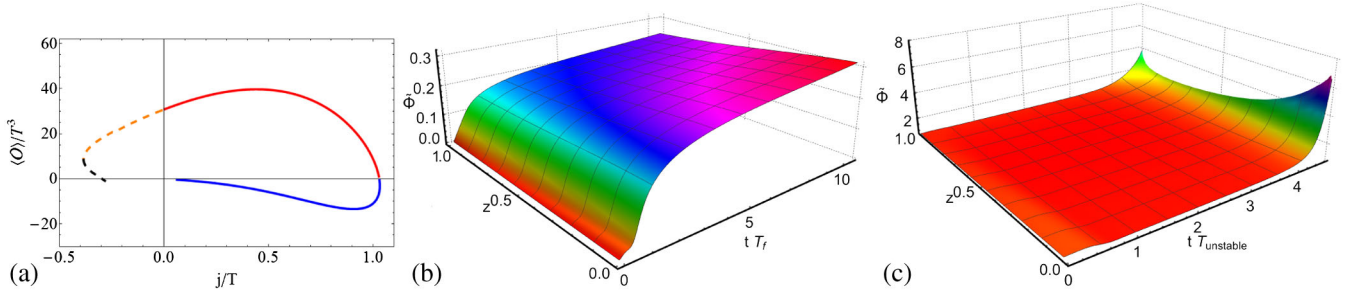

FIG. 3. (a) We show the expectation of the scalar operator as a function of the source over the temperature for both the stable (blue) and unstable (red) phase. There are also two other branches shown dashed, which we comment on in Sec. III. (b) For the maximum source, the equilibration time diverges, and the system equilibrates in a time $\gg 1/T$. (c) When evolving initial data slightly different from Fig. 1, the coefficient of the unstable QNM changes sign, and the solution grows instead of decreasing at late times.

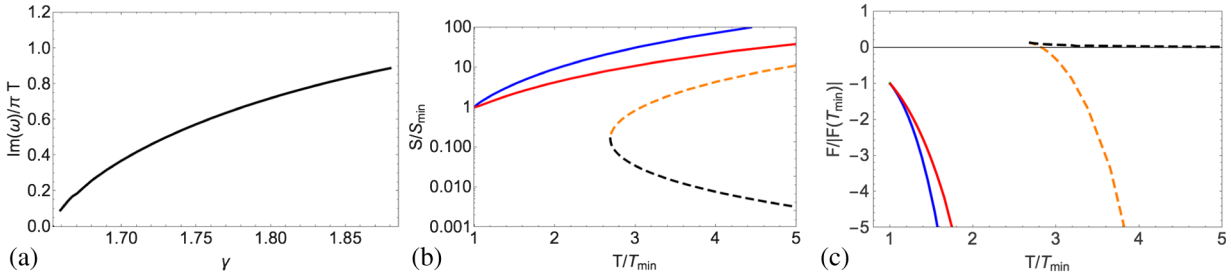

FIG. 4. (a) We show the unstable QNM as a function of γ. It is especially interesting that the relaxation time diverges as γ approaches the critical value from above. (b, c) We show the entropy and free energy as a function of the temperature over the minimum temperature found for fixed source j. Both curves are normalized with their value at the minimum temperature. Interestingly, both the dynamically unstable (red) and stable (black) black brane phases have positive specific heat. Third and fourth branches are shown dashed, which smoothly connect to the thermal gas phase for high temperature, whereby as usual the small branch has negative specific heat.

temperature of the final state, which is an interesting novelty for nonconformal strongly coupled systems.

Lastly, we studied the unstable QNM at $j = 0$ for different values of γ, which is presented in Fig. 4(a). As γ approaches the critical value 1.65 from above, the imaginary part goes to zero, and we hence again find a diverging relaxation time. We also verified that for smaller γ no instability is present at zero momentum.

We performed several numerical checks. All our simulations satisfy the constraint equation to better than 10^{-5} precision [with the exception of Fig. 3(c)]. We also compared the QNM spectrum with fits of the dynamical evolution when this was in the linear regime, which is a nontrivial check. Lastly, we used a thermodynamic code to construct the time-independent solution, which allowed us to study the equilibrium properties of both the stable and unstable solutions.

III. DISCUSSION

The thermodynamics of the stable and unstable phase is presented in Fig. 4(b) and 4(c), where we show the entropy and free energy vs the temperature (computed using the method of Ref. [44]). Indeed, the unstable solution has smaller entropy than the stable solution, but this phase still consists of a large black hole, in the sense that the black hole grows [45]. This stands in contrast with two other branches in our model, shown dashed, which includes a small black hole branch, smoothly connecting to the thermal gas phase as the temperature goes to infinity. These branches are more involved to study dynamically as they are thermodynamically unfavored, and we plan to report on this in future work.

As alluded to in the Introduction, one curious feature is that the solution shown in Fig. 1(a) is unstable already at zero momentum, in contrast to the standard Gregory-Laflamme type instability. This in particular allows for a positive specific heat and a positive speed of sound squared, as can be inferred from Fig. 4(c). From a field theory point of view, this instability is perhaps less dramatic, as the plasma need not break up, but evolves homogeneously to a different phase. Nevertheless, the scalar operator acquires a different expectation value, and the entropy can at least double for small j.

Our results are very generic. For other dimensions, other scaling dimensions and other potentials with a large enough ϕ^4 contribution, we were able to find the unstable QNM at zero momentum. Also, the inclusion of anisotropy in the metric (4) does not give rise to qualitative changes.

The unstable QNM found in Fig. 1 has an interesting alternative. When choosing $\tilde{\Phi}(z,t) = 1.06823$ instead of

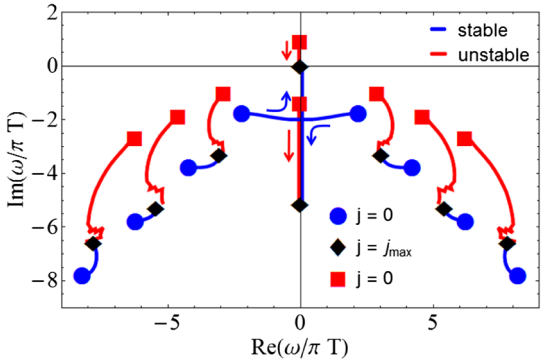

FIG. 5. Here, the first eight QNMs of Fig. 2 are shown on the complex plane as a function of j. The lowest stable QNM (blue) hits the imaginary axis at $j/T = 0.95$, after which the modes separate on the axis to meet the unstable QNMs at $j = j_{\max}$.

$\tilde{\Phi}(z,t) = 1.06822$, the coefficient of the unstable QNM changes sign, and hence $f_3(t)$ starts growing exponentially instead of decreasing. This means the final stable configuration found in Fig. 1 will not be reached. Our numerics do not allow us to determine the final end point of this type of evolution, of which the first moments are displayed in Fig. 5(c). This evolution would be interesting for future study, whereby we note that our evolution starts with regular initial conditions, an apparent horizon and that our model satisfies the null energy condition.

Our results are most easily understood in terms of the QNM spectrum of both the stable (blue) and unstable solutions (red) on the complex plane, which we show as a function of j again for $\gamma = 4\sqrt{2}/3$ in Fig. 5. Starting at the blue circle for large black holes with $j = 0$, each QNM follows a blue trajectory until the maximum source $j = j_{\max}$. At this point, the lowest QNM hits the origin, and we show the other branch in red, ending again at $j = 0$ with a red square. It is interesting to see the lowest QNM of the stable phase hits the imaginary axis and hence becomes overdamped, which is similar to QNMs in Lifshitz spacetimes [15].

Indeed, nonconformal theories contain rich physics. The different black brane solutions found contain a new dynamical instability already at zero momentum. This new mechanism leads in particular to a value of j/T where the quasinormal mode frequency goes to zero and hence the relaxation time diverges, which we showed to be a generic feature in nonconformal strongly coupled theories.

ACKNOWLEDGMENTS

We thank Alex Buchel, Steven Gubser, Phil Szepietowski, Takaaki Ishii, Luis Lehner, Michal Heller, Elias Kiritsis, David Mateos, Francesco Nitti, and Chris Rosen for useful discussions. W. S. is supported by the U.S. Department of Energy under Grant No. DE-SC0011090. This work was supported by the Netherlands Organisation for Scientific Research under VIDI Grant No. 680-47-518 and the Delta-Institute for Theoretical Physics that is funded by the Dutch Ministry of Education, Culture and Science.

Note added.—While finalizing our draft, the paper [9] that also reports dynamical instability at vanishing momentum in a similar gravitational setting appeared on the arXiv. However, the QNM they find has a small positive imaginary part, about 0.05.

[1] P. M. Chesler and L. G. Yaffe, Phys. Rev. Lett. **102**, 211601 (2009).
[2] P. M. Chesler and L. G. Yaffe, Phys. Rev. Lett. **106**, 021601 (2011).
[3] M. P. Heller, R. A. Janik, and P. Witaszczyk, Phys. Rev. Lett. **108**, 201602 (2012).
[4] M. P. Heller, D. Mateos, W. van der Schee, and D. Trancanelli, Phys. Rev. Lett. **108**, 191601 (2012).
[5] T. Ishii, E. Kiritsis, and C. Rosen, J. High Energy Phys. 08 (2015) 008.
[6] A. Buchel, M. P. Heller, and R. C. Myers, Phys. Rev. Lett. **114**, 251601 (2015).
[7] J. F. Fuini and L. G. Yaffe, J. High Energy Phys. 07 (2015) 116.
[8] R. A. Janik, G. Plewa, H. Soltanpanahi, and M. Spalinski, Phys. Rev. D **91**, 126013 (2015).
[9] R. A. Janik, J. Jankowski, and H. Soltanpanahi, J. High Energy Phys. 06 (2016) 047.
[10] U. Gursoy, M. Jarvinen, and G. Policastro, J. High Energy Phys. 01 (2016) 134.
[11] Y. Du, S.-Q. Lan, Y. Tian, and H. Zhang, J. High Energy Phys. 01 (2016) 016.
[12] M. Attems, J. Casalderrey-Solana, D. Mateos, I. Papadimitriou, D. Santos-Oliván, C. F. Sopuerta, M. Triana, and M. Zilhão, arXiv:1603.01254.
[13] W. Sybesma and S. Vandoren, J. High Energy Phys. 05 (2015) 021.
[14] J. Brewer and P. Romatschke, Phys. Rev. Lett. **115**, 190404 (2015).
[15] U. Gursoy, A. Jansen, W. Sybesma, and S. Vandoren, Phys. Rev. Lett. **117**, 051601 (2016).
[16] U. Gursoy and E. Kiritsis, J. High Energy Phys. 02 (2008) 032.
[17] U. Gursoy, E. Kiritsis, and F. Nitti, J. High Energy Phys. 02 (2008) 019.
[18] C. Csaki and M. Reece, J. High Energy Phys. 05 (2007) 062.

[19] S. S. Gubser, A. Nellore, S. S. Pufu, and F. D. Rocha, Phys. Rev. Lett. **101**, 131601 (2008).
[20] S. S. Gubser and A. Nellore, Phys. Rev. D **78**, 086007 (2008).
[21] U. Gursoy, E. Kiritsis, L. Mazzanti, and F. Nitti, Phys. Rev. Lett. **101**, 181601 (2008).
[22] U. Gursoy, E. Kiritsis, L. Mazzanti, and F. Nitti, Nucl. Phys. **B820**, 148 (2009).
[23] R. A. Konoplya and A. Zhidenko, Rev. Mod. Phys. **83**, 793 (2011).
[24] R. Gregory and R. Laflamme, Phys. Rev. Lett. **70**, 2837 (1993).
[25] S. Hawking, Commun. Math. Phys. **43**, 199 (1975).
[26] H. S. Reall, Phys. Rev. D **64**, 044005 (2001).
[27] S. S. Gubser and I. Mitra, arXiv:hep-th/0009126.
[28] S. S. Gubser and I. Mitra, J. High Energy Phys. 08 (2001) 018.
[29] V. E. Hubeny and M. Rangamani, J. High Energy Phys. 05 (2002) 027.
[30] A. Buchel, Nucl. Phys. **B731**, 109 (2005).
[31] A. Buchel, Nucl. Phys. **B820**, 385 (2009).
[32] S. Hollands and R. M. Wald, Commun. Math. Phys. **321**, 629 (2013).
[33] J. J. Friess, S. S. Gubser, and I. Mitra, Phys. Rev. D **72**, 104019 (2005).
[34] It is an interesting question if a dynamical instability also implies a thermodynamic instability. Naively, our example is thermodynamically stable with respect to all conserved charges, but as noted in Ref. [33], it may be more natural to consider a wider definition of thermodynamics which includes nonconserved charges.
[35] H. Bondi, Nature (London) **186**, 535 (1960).
[36] W. van der Schee, Ph.D. thesis, Utrecht University, 2014, arXiv:1407.1849.
[37] S. de Haro, S. N. Solodukhin, and K. Skenderis, Commun. Math. Phys. **217**, 595 (2001).
[38] P. K. Kovtun and A. O. Starinets, Phys. Rev. D **72**, 086009 (2005).
[39] P. Benincasa, A. Buchel, and A. O. Starinets, Nucl. Phys. **B733**, 160 (2006).
[40] To obtain the QNM spectrum, we need the (time-independent) background solution. This can be directly obtained from our dynamical evolution when the background metric is changing slowly enough. Alternatively, we also solved the time-independent Einstein equations for the metric (4) directly, which can easily be done numerically using Mathematica.
[41] L. G. Yaffe, http://msstp.org/?q=node/289.
[42] We chose this value because this is the maximum value where the spectrum of fluctuations around the vacuum is still well defined [17].
[43] In practice, this fine-tuning is done by increasing $f_3(0)$; for values higher than the fine-tuned value, the evolution looks like Fig. 3(c), which is easy to distinguish from Fig. 1(a) at late times and hence makes a binary search algorithm straightforward. Note that we have to fine tune the coefficient of one QNM, so we just have to fine tune one parameter instead of a function.
[44] U. Gursoy, E. Kiritsis, L. Mazzanti, and F. Nitti, J. High Energy Phys. 05 (2009) 033.
[45] There is a tiny branch in between these two: the minimum entropy and temperature do not occur at the exact same point, and that tiny branch has negative specific heat, but no instability at zero momentum yet.